Astronomy & Astrophysics manuscript no. paper
(DOI: will be inserted by hand later)
May 26, 2005

Magnetic turbulence in cool cores of galaxy clusters

Torsten A. Enßlin[1] and Corina Vogt[1,2]

[1] Max-Planck-Institut für Astrophysik, Karl-Schwarzschild-Str.1, Postfach 1317, 85741 Garching, Germany
[2] ASTRON, P.O.Box 2, 7990 AA Dwingeloo, The Netherlands

May 26, 2005

Abstract. We argue that the recently reported Kolmogorov-like magnetic turbulence spectrum in the cool core of the Hydra A galaxy cluster (Vogt & Enßlin 2005) can be understood by kinetic energy injection by active galaxies which drive a turbulent non-helical magnetic dynamo. We develop an analytical model of the turbulence in cool cores and show that it fits well to Faraday rotation magnetic field measurements and others like minimum energy estimates for a number of cool core clusters. Moreover, our model allows predictions for magnetic fields in clusters in which the appropriate observational information is still missing, it allows predictions for yet unobserved quantities like the hydrodynamical turbulence velocity and characteristic length-scale, and suggests some level of magnetic intermittency and large-scale hydrodynamic viscosity. Furthermore, the success of the model to explain the field strength in cool core clusters suggests that in general cluster magnetic fields are directly reflecting hydrodynamical turbulence, also in clusters without cool cores.

Key words. Galaxies: cluster: general – cooling flows – Magnetic Fields – Turbulence – X-rays: galaxies: clusters – intergalactic medium

1. Introduction

1.1. Magnetic fields in cool cores

Galaxy clusters contain magnetised plasma on cluster scales, as radio-synchrotron emission of relativistic electrons reveals in form of the so-called *cluster radio halos*. The origin, the strength and geometry of these magnetic fields is still a mystery.

With the emerging of the first theories of magnetic dynamos (Zeldovich et al. 1990), it was proposed that the cluster magnetic fields are the product of turbulence acting on a seed magnetic field. The seed field could be a remnant of non-equilibrium processes in the early Universe, or due to some weak magnetisation caused by galactic outflows in form of winds and radio plasma (for a review see Widrow 2002).

Initially, wakes of the weakly sonic galaxy motions were thought to be the main driver of the intra-cluster turbulence (e.g. Jaffe 1980; Roland 1981; Ruzmaikin et al. 1989). However, it was realised using numerical simulations of large-scale structure formation that the violent mergers of galaxy clusters are a much more powerful source of turbulence (e.g. Tribble 1993).

It was therefore a surprise when it was found that the strongest magnetic fields seem to be located in the centres of clusters which were dynamically the most relaxed, since the last major merger was long ago. These *cooling flow* (now *cool core*) clusters had time to develop a cool, dense central region due to the cooling instability of optically thin X-ray emission of cooling gas. The magnetic fields reported for those cooling flow regions inferred by Faraday rotation studies were extraordinary strong (up to 50 μG) compared to the few μG fields reported for non-cooling flow clusters (for recent reviews see Carilli & Taylor 2002; Govoni & Feretti 2004). It was speculated, that the strong fields could be a result of the compressional flow in the cooling flow (Soker & Sarazin 1990).

However, Chandra and XMM observations revealed that the standard cooling flow picture, in which unheated gas cools down to neutral gas temperatures, must be incorrect, since the expected amount of line emission of cold ($<$ 0.3 keV) gas or the expected number of stars formed from the condensing gas was not detected[1]. Therefore a heat source has to be present which balances the cooling of the coldest gas. Since the theoretical scenario associated with the term *cooling flow* has been ruled out recently, the solely observationally motivated term *cool core* is used in the following.

The energy losses of the cool core have to be balanced by a similar energy injection. There were two main proposals[2] for the heat source in cool cores:

(i) Thermal conductivity, which is close to Spitzer's estimate, and therefore not suppressed by magnetic fields. This

[1] Heckman et al. (1989); Fabian et al. (1991); Hansen et al. (1995); Allen (1995); Jaffe & Bremer (1997); Smith et al. (1997); O'Dea et al. (1998); Crawford et al. (1999); Donahue et al. (2000); Edge (2001); Oegerle et al. (2001); Salomé & Combes (2003); Edge & Frayer (2003)

[2] There are also other mechanisms discussed in the literature, e.g. the influence of a cosmic ray population (Chandran 2004; Cen 2005).

would allow the inward transport of heat from the hotter environmental intra-cluster medium (ICM)[3].

(ii) Dissipation of mechanical energy released by the expansion and buoyant motion of radio bubbles inflated by the radio galaxies which are typically found in the centre of a cool core of a galaxy cluster[4].

The thermal conduction scenario (i) as the only heat injection mechanism into cool cores faces severe problems in terms of fine-tuning the required energy injection, and explaining the existence of cold gas clouds which need sufficient insulation from the keV gas (Soker 2003; Nipoti & Binney 2004). Too strong conduction would erase the cool core, but too weak conduction can not prevent the cooling catastrophe. Therefore a conductively heated cool core should be unstable.

The scenario (ii) in which the central radio galaxy balances the radiative energy losses of the cool core provides naturally fine tuning in form of a self-adapting feedback mechanism: If the radio galaxy activity is triggered by cold gas condensing out of the cool core onto the central galaxy, the galaxy activity increases until it disrupts further accretion (Churazov et al. 2001).

In this work we assume scenario (ii), not only since it is – at least in our view – theoretically more compelling, but also because it predicts a certain level of hydrodynamical turbulence, which can be compared to the level required to explain the cool core magnetic fields by magnetic dynamo theory.

There have been some reports on observed signatures of turbulent flows in cool cores of galaxy clusters, and the scenario (ii) investigated here seems to become widely accepted, at least as a working hypothesis (e.g. Loewenstein & Fabian 1990; Churazov et al. 2001; Böhringer et al. 2002; Churazov et al. 2002, 2004).

1.2. Observations of cluster magnetic fields

Magnetic fields in normal clusters and cool core clusters have revealed their existence by the diffuse radio halo emission in many clusters and radio mini-halos in cool core regions. Furthermore, the Faraday rotation of linearly polarised radio emission traversing the intra-cluster medium proves independently the existence of intra-cluster magnetic fields. If the Faraday active medium is external to the source of the polarised emission, one expects the change in polarisation angle to be proportional to the squared wavelength. The proportionality factor is called the rotation measure (*RM*). This quantity can be evaluated in terms of the line of sight integral over the product of the electron density and the magnetic field component along the line of sight.

Magnetic fields in non-cool core clusters of galaxies detected through Faraday rotation measurements are of the order of a few μG. Kim et al. (1991) measured field strengths of about 2 μG on scales of 10 kpc in a statistical sample of point sources observed through the Coma cluster. Clarke et al. (2001); Clarke (2004); Johnston-Hollitt & Ekers (2004) derive similar field strengths of several μG in various samples of point sources observed within and through various low redshift clusters in the northern and southern hemisphere. The analysis of *RM* maps of extended radio sources have lead to the same conclusion (e.g. Feretti et al. 1995, 1999; Taylor et al. 2001; Govoni et al. 2001; Eilek & Owen 2002; Vogt & Enßlin 2003).

However, the analysis of Faraday rotation measurements of extended radio sources in the centre of cool core clusters reveal higher magnetic field strengths. Such an analysis has been done for the Centaurus cluster by Taylor et al. (2002), for A1958 (better known as 3C295) by Perley & Taylor (1991), for A1795 by Ge & Owen (1993), for Cygnus A by Dreher et al. (1987) and for Hydra A by Taylor & Perley (1993). From these *RM* measurements, magnetic field strengths of 10 to 40 μG have been reported for the cores of these cool core clusters on scales of 3–5 kpc.

These rather large field values for cool core clusters have been revised in the case of Hydra A by a recent analysis of the observational data. A high quality Faraday rotation map of the north lobe of Hydra A produced by the novel PACERMAN algorithm (Dolag et al. 2005; Vogt et al. 2005) based on the data of Taylor & Perley (1993) was analysed by Vogt & Enßlin (2005). They used a maximum likelihood estimator for the derivation of the magnetic power spectra, based on the theory of turbulent Faraday screens (Enßlin & Vogt 2003; Vogt & Enßlin 2003), and also using the most up-to date gas density profile of the cool core, which turned out to make a crucial difference. Thereby, a magnetic field strength of $7\pm2\mu$G was found in the centre of the cool core region of the Hydra A cluster, which is still a significantly larger field than reported for non-cool core clusters. Vogt & Enßlin (2005) measured the detailed magnetic power spectrum from the Hydra A dataset, which revealed a Kolmogorov-type spectrum on small scales indicating turbulence (see Fig. 1).

It has been debated, if the magnetic fields seen by the Faraday effect exist on cluster scales in the ICM, or in a mixing layer around the radio plasma which emits the polarised emission (Bicknell et al. 1990; Rudnick & Blundell 2003). However, there is no valid indication of a source local Faraday effect in the discussed cases (Enßlin et al. 2003), and the Faraday rotation signal excess of radio sources behind clusters compared to a field control sample strongly supports the existence of strong magnetic fields in the wider ICM (Clarke et al. 2001; Johnston-Hollitt & Ekers 2004; Clarke 2004).

1.3. Structure of the paper

The paper is structured as follows: In Sect. 2 we introduce the turbulent dynamo and summarise its expected and observed

[3] Malyshkin (2001); Narayan & Medvedev (2001); Voigt et al. (2002); Ruszkowski & Begelman (2002); Cho et al. (2003); Soker et al. (2004); Voigt & Fabian (2004); Soker (2004); Jubelgas et al. (2004); Chandran & Maron (2004)

[4] Churazov et al. (2001); Brüggen & Kaiser (2001); Quilis et al. (2001); Brüggen et al. (2002); Chandran (2004); Hoeft & Brüggen (2004); Dennis & Chandran (2005). There have been also observations of hot gas bubbles (Mazzotta et al. 2004), which may also contribute to the cool core heating in a very similar way as the radio bubbles (Soker & Pizzolato 2005)

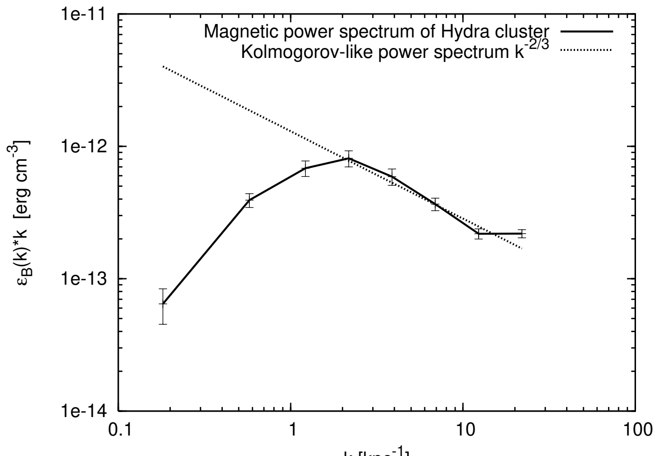

Fig. 1. Magnetic turbulence in the centre of the cool core cluster Hydra A as derived from the Faraday rotation map of the northern radio lobe of Hydra A by Vogt & Enßlin (2005). An angle of 45° was assumed in this figure between the line of sight and the approaching north-lobe. Variation of this angle changes the overall normalisation of the spectrum, but not its shape. The right-most data point is likely to be contaminated by observational noise in the Faraday map. A central root-mean-square magnetic field strength of $B_{\rm rms} = 7.3 \pm 0.2 \pm 2\,\mu$G and a magnetic autocorrelation length of $\lambda_B = 2.8 \pm 0.2 \pm 0.5$ kpc was derived by Vogt & Enßlin (2005). The first errors are the statistical uncertainties due to the limited statistics, whereas the systematic error is reflecting the uncertainties in the geometry of the radio source and the Faraday screen.

signatures in galaxy clusters, mainly based on the above mentioned estimate of the magnetic power-spectrum in the Hydra A cluster core. In Sect. 3 we develop a steady-state analytical description of the expected magnetic turbulence due to the stirring motion of buoyant radio bubbles from the central galaxy, which is assumed to regulate the energy content of the cool core. This is applied in Sect. 4 to a number of prominent cool core clusters, and compared to existing information on magnetic fields whenever available. Sect. 5 contains our conclusions.

Throughout the paper, we assume a Hubble constant of $H_0 = 70$ km/s/Mpc, and translate literature values of luminosities, length scales, electron densities and magnetic field strengths derived from Faraday rotation measurements to this value without further notice.

2. Turbulent magnetic dynamo

2.1. Concepts

The Kolmogorov-like magnetic power spectrum in the cool core of the Hydra A cluster indicates that the magnetic fields are shaped and probably amplified by hydrodynamical turbulence (e.g. De Young 1992). Therefore, it seems most promising to seek the origin of the observed magnetic power spectrum in the theories of turbulent dynamos. Note, that a very similar view and approach are used in the recent work by Subramanian et al. (2005), in which the magnetic fields in non-cooling core clusters were also assumed to be maintained by turbulence. In that environment the turbulence is due to merger events and galaxy motions, whereas here it is due to the inflation and buoyant motion of radio bubbles.

Since cool cores of galaxy clusters are not believed to rotate, the gas flow is probably non-helical and the galactic dynamo theories do not apply here. Instead, the non-helical turbulent dynamo (also called small-scale dynamo) should operate if the gas flow is sufficiently random, as it would be in the case of developed turbulence.

The random gas motion would stretch and fold any initial seed magnetic fields and lead to an exponential growth of the magnetic energy density with time with the characteristic time-scale being the eddy-turnover time. This proceeds as long as the dynamical back-reaction of the magnetic field is unimportant. The folding operations of the flow form small-scale magnetic reversals perpendicular to the local field directions (Schekochihin et al. 2002). Magnetic diffusivity limits the scales to be of the order of $\lambda_B \sim \lambda_{\rm T} R_{\rm m}^{-1/2}$, where $\lambda_{\rm T}$ is the turbulence injection scale, and $R_{\rm m}$ is the magnetic Reynolds-number (Ruzmaikin et al. 1989). The typical bending radius of the fields should be of the order of the turbulence length-scale $\lambda_{\rm T}$.

As soon as the Lorentz-force becomes sufficiently strong, the fields do not follow the flow passively, but start to try to disentangle themselves. This back-reaction motion leads to an increase in the effective magnetic diffusivity, and therefore to a lower, renormalised magnetic Reynolds-number implying fields to become organised on larger scales. The Reynolds-number decreases until it reaches a critical value $R_{\rm c} \sim 10-100$, below which the turbulent dynamo would stop to operate. The system reaches a saturated state, in which the magnetic correlation length scale $\lambda_B \sim \lambda_{\rm T} R_{\rm c}^{-1/2}$ is solely determined by the turbulence length scale and the critical Reynolds number.

In the picture initially developed by Zeldovich et al. (1990), the magnetic fields are highly intermittent: only a small fraction f_B of the volume is actually strongly magnetised, whereas the remaining volume $1 - f_B$ does not carry dynamically important magnetic fields. Zeldovich et al. (1990) and others (Ruzmaikin et al. 1989; Sokolov et al. 1990; Subramanian 1999) assumed the magnetised regions to be organised as magnetic flux ropes of volume $\lambda_{\rm T}\,\lambda_B^2$ per eddy volume $\lambda_{\rm T}^3$. The occupied volume fraction would be $f_B \sim \lambda_B^2/\lambda_{\rm T}^2 \sim R_{\rm c}^{-1}$. Numerical simulations indicate that the magnetic structures are more sheet-like with thickness λ_B (Brandenburg & Subramanian 2004), leading to a $f_B \sim \lambda_B/\lambda_{\rm T} \sim R_{\rm c}^{-1/2}$ as assumed in Subramanian et al. (2005). In order to allow for any geometry of the magnetic structures in the saturated state, we assume that they are effectively d-dimensional, giving

$$f_B \sim \frac{\lambda_{\rm T}^d\,\lambda_B^{3-d}}{\lambda_{\rm T}^3} \sim R_{\rm c}^{-\frac{3-d}{2}}\,,\ \text{with } 1 \le d \le 3. \tag{1}$$

Under the steady-state conditions of the saturated dynamo, the hydrodynamical dissipation of turbulent energy on scale $\lambda_{\rm T}$ and the relaxation of magnetic structures bent on the same scales $\lambda_{\rm T}$ should have the same time scales:

$$\tau_B \sim \frac{\lambda_{\rm T}}{v_{\rm A}^{\rm struct.}} = \lambda_{\rm T}\sqrt{\frac{\rho}{2\,\varepsilon_B^{\rm struct.}}} \tag{2}$$

$$\tau_{\rm T} \sim \frac{\lambda_{\rm T}}{{\rm v_T}} = \lambda_{\rm T}\sqrt{\frac{\rho}{2\,\varepsilon_{\rm T}}}\,, \tag{3}$$

where $v_A^{\rm struct.}$ and $\varepsilon_B^{\rm struct.}$ are the Alfvénic velocity and energy density within the magnetic structures, and v_T and ε_T the turbulent velocity and energy density, respectively. Then $\tau_B \sim \tau_T$ implies that the magnetic fields within the structures are in equipartition with the environmental turbulent energy density, and the volume averaged magnetic energy density is therefore lower than these by the magnetic volume filling factor:

$$\varepsilon_B \sim \varepsilon_B^{\rm struct.}\, f_B \sim \varepsilon_{\rm T}\, f_B \sim \varepsilon_{\rm T}\, R_{\rm c}^{-\frac{3-d}{2}}\,. \tag{4}$$

Thus, with the knowledge or assumption of the critical Reynolds-number R_c, and the effective dimensionality d of the magnetised regions it is possible to translate properties of the hydrodynamical turbulence to the magnetic turbulence and vice versa, under the assumption that the system is in the saturated dynamo state.

In the numerical examples, we will investigate two scenarios of magnetic topology:

1. Magnetic fields mostly organise in flux tubes ($d = 1$, $R_c = 20$, $\Rightarrow$ $f_B = 0.05$). This scenario reflects the original assumption on turbulent magnetic structures by Zeldovich et al. (1990). Here we consider it to investigate the induced hydrodynamical viscosity on large scales, since there are published predictions for this quantity in the flux rope scenario (Longcope et al. 2003).
2. Magnetic fields mostly organise in sheets and ribbons ($d = 2$, $R_c = 35$, $\Rightarrow$ $f_B = 0.17$). This scenario is more in agreement with recent numerical simulations, as argued by Subramanian et al. (2005).[5]

The scaling of any quantity with the parameters R_c and d will also be provided, so that this theory may stay applicable even in case the adopted values need readjustments.

2.2. Magnetic viscosity

In the saturated dynamo state, the magnetic fields are not passively following the hydrodynamical flow of the bulk motion, but possess an independent velocity component due to the Lorentz force. This should lead to a slippage of strongly and weakly magnetised regions relative to each other, possibly causing some friction due to induction of small scale eddies in the wakes of the magnetic structures. For the flux rope dynamo scenario, Longcope et al. (2003) give the expected viscosity on large spatial scales in the saturated state to be of the order of 4% of the turbulent diffusivity $\kappa_T \approx v_T\ \lambda_T/3$, thus

$$\kappa_{\rm visc} \approx 0.04\,\frac{{\rm v_T}\,\lambda_{\rm T}}{3}\,. \tag{5}$$

Also in the scenario of mainly 2-dimensional magnetic structures, one would expect such viscous effects, but no estimates of the viscosity exist to our knowledge.

2.3. Signatures

According to the scenario described above, the magnetic fields in the turbulent cool cores of galaxy clusters should exhibit the following properties:

A. The magnetic power spectrum should reflect the hydrodynamical power spectrum, just with a lower normalisation and on smaller spatial scales. That means that a Kolmogorov-inertial range power law behaviour of hydrodynamical turbulence should also be found in the magnetic spectrum
B. The average magnetic energy density ε_B is lower than the turbulent kinetic energy density $\varepsilon_{\rm kin}$ by $\varepsilon_B \approx \varepsilon_{\rm kin}\, f_B$, where $f_B \sim R_c^{-(3-d)/2} \sim 0.05\ldots0.2$ depending on the critical magnetic Reynolds number and the dimensionality of the magnetic structures.
C. The magnetic fluctuations are concentrated on a perpendicular scale λ_B, which is smaller than the hydrodynamical turbulence injection scale λ_T by $\lambda_B \approx \lambda_T R_c^{-1/2}$.
D. Magnetic correlations exist up to a scale λ_T, turn there into an anti-correlation as a consequence of $\boldsymbol{\nabla}\cdot\boldsymbol{B} = 0$, and quickly decay on larger scales.
E. The fields may be spatially intermittent. This may be understood by Zeldovich's flux rope model, in which magnetic ropes with diameter λ_B are bent on scales of the order λ_T. Alternatively, also supported by recent numerical simulations, it can be understood in terms of magnetic sheets of thickness λ_B and size λ_T.
F. In case of intermittent fields, the field strength within the magnetic structures should be in energy equipartition with the average turbulent kinetic energy density of their environment.
G. The magnetic drag of such intermittent structures produces a hydrodynamical viscosity on large scales. In case of the Zeldovich-flux rope scenario, an estimate of a viscosity of 4% of the turbulent diffusivity $\kappa_T \approx v_T\ \lambda_T/3$ was made by Longcope et al. (2003).

2.4. Observations

We investigate briefly if the above predictions of the non-helical dynamo theory are in agreement with observations.

A. A Kolmogorov-like magnetic power spectrum in a cluster cool core is revealed by the Faraday rotation map of Hydra A (Vogt & Enßlin 2005).
B. Translating the Faraday-rotation based estimate of the magnetic energy density to the expected turbulent energy density $\varepsilon_T \sim \varepsilon_B/f_B$ in the Hydra A cluster yields

[5] Haugen et al. (2004) investigate numerically magnetic turbulence in the case of a Prandtl of order unity, and find a magnetic to turbulent energy ratio of the order of $f_B \approx 0.4$ in this regime. Since they report a $R_c \approx 35$, their case could be described by $d = 2.5$ dimensional magnetic intermittency. However, as Dennis & Chandran (2005) point out, the dissipation rate of turbulent energy seems to be doubled compared to not (or less) magnetised scenarios, which would lead to a reduction in the turbulent and magnetic energy densities by a similar factor. For the observables of the magnetic fields, like field strength, length, and Faraday signal, there would be very little numerical difference to the $d = 2$ scenario. For this reason, we do not follow this scenario separately, but assume it to be sub-summed under the $d = 2$ case.

$0.3 \ldots 1.0\,10^{-10}\,\mathrm{erg\,cm^{-3}}$, which corresponds to turbulent velocities of $v_{\rm turb} \approx 250 \ldots 430\,\mathrm{km/s}$. This is comparable to velocities of buoyant radio plasma bubbles Enßlin & Heinz (2002), which are expected to stir up turbulence (e. g. Churazov et al. 2001).

C. The expected turbulence injection scale in the Hydra A cluster core is of the order of $\lambda_{\rm T} \sim \lambda_B\, R_{\rm c}^{1/2} \sim 10 \ldots 20$ kpc, again consistent with the radio plasma of Hydra A being the source of turbulence, since turbulence injection scale and the radio lobes of Hydra A have comparable dimensions. The dynamical connection of the radio source length scale and the magnetic turbulence scale would explain why the Faraday map of Hydra A is conveniently sized to show us the peak of the magnetic power spectrum (see Fig. 1).

D. The expectation of weak magnetic fluctuations on scales larger than the turbulence injection scale is hard to test with the available data due to the limited size of the *RM* map used. However, the downturn of the magnetic power spectrum at small k-values visible in Fig. 1 is in agreement with the requirement of magnetic anti-correlations on large scales.

E. Magnetic structures in form of flux ropes or ribbons might have been detected as stripy patterns in the *RM* map of 3C465 (Eilek & Owen 2002), in support of the assumed intermittence of the small-scale dynamo .

F. The fraction of strongly magnetised volume may be as small as $f_{\rm B} = R_{\rm c}^{-1} \approx 0.05 \ldots 0.2$. Strongly intermittent fields in galaxy clusters may help to reconcile the discrepancy between Faraday and inverse Compton based magnetic field estimates (Enßlin et al. 1999). The latter estimate could easily be biased to low field regions due to the faster removal of ultra-relativistic electrons in strong field regions by synchrotron emission.

G. The expected hydrodynamical viscosity on large scales in the Hydra cluster is of the order of $10^{28}\,\mathrm{cm^2/s}$ (if the estimate in Eq. 5 based on the flux rope picture is applicable). It is interesting to note, that Fabian et al. (2003b) argue for the comparable Perseus cluster cool core for a lower limit on the large scale viscosity of $4 \cdot 10^{27}\,\mathrm{cm^2/s}$. They base their arguments on the observation of very elongated H-α filaments which suggest a laminar flow pattern behind buoyantly rising radio bubbles. An upper limit on the viscosity in the (non-cooling core) Coma cluster of $\sim 3 \cdot 10^{29}\,\mathrm{cm^2/s}$ is reported by Schuecker et al. (2004). Both limits are consistent with our coarse estimate of the large scale viscosity and enclose it. However, it should be pointed out that the presence of a significant viscosity, as well as the underlying magnetic intermittency, in galaxy clusters should be regarded as being speculative, and not directly confirmed by observations.

3. Magneto-Hydrodynamical turbulence in cool cores

3.1. Scope of the approach

A theoretical model of the magneto hydrodynamical turbulence in cool cores of galaxy clusters is developed in the following. The model is intended to capture the most essential features of the physical picture. We do not attempt to make accurate numerical predictions, but hope to get insight into the scaling-relations of the different quantities and their order of magnitude values.

Although cool cores exhibit a structured gas distribution, for our order-of-magnitude calculation we describe them as quasi-homogeneous spheres. We briefly present a radial extension of our model in Sect. 3.7.

The episodic injection of radio plasma by the central galaxy into cool cores should lead to temporal variations of the state of the core. Nevertheless, we treat the system as being in a steady state. Our estimates provide therefore only approximate temporal mean values. Observations of cool cores will always show snapshots of the cool core evolution. Thus, deviations between our predictions and the observed state of individual cool cores should not be too surprising.

Detailed numerical modelling of the processes would be required to overcome our simplifying assumptions which is well beyond the scope of this initial investigation of the scenario presented here.

3.2. A simplified cool core description

A cool core is a condensation of cold gas of mass $M_{\rm cc}$, which dropped out of the hot phase of a galaxy cluster due to the faster radiative cooling of denser gas. The observables of the cool core, which can be used for diagnostics of the physical parameters, are the bolometric X-ray luminosity of the cool core $L_{\rm cc}$, its temperature $T_{\rm cc}$, and its radius $r_{\rm cc}$ from which the central electron density $n_{\rm cc}$ can be deduced.

The energy feedback of the central radio source prevents the cool core gas from falling below a characteristic temperature $T_{\rm cc} \sim \mathrm{keV}$[6], which is given by the requirement that the atomic line emission does not dominate. Otherwise, in the case of a lower temperature, the gas in the cool core would rapidly condense onto the central galaxy due to a cooling catastrophe driven by emission-lines. The pressure in a cool core is

$$P_{\rm cc} = 2\, n_{\rm cc}\, T_{\rm cc}\,, \tag{6}$$

where we ignore here and in the following the presence of any element heavier than Hydrogen in pressure and mass terms for simplicity. The cool core gas mass is therefore

$$M_{\rm cc} = n_{\rm cc}\, m_{\rm p}\, V_{\rm cc}\,, \text{ where } V_{\rm cc} = \frac{4\,\pi}{3} r_{\rm cc}^3\,. \tag{7}$$

The X-ray luminosity of the cool core is given by

$$L_{\rm cc} = \Lambda_{\rm X}(T_{\rm cc})\, n_{\rm cc}^2\, V_{\rm cc}\,, \tag{8}$$

where

$$\Lambda_{\rm X}(T_{\rm cc}) = \Lambda_0\, T_{\rm cc}^{\frac{1}{2}} + \Lambda_{\rm lines}(T_{\rm cc}) \tag{9}$$

consists of a Bremsstrahlung- and a line emission term. The line emission term should be at best comparable to the

[6] We express temperatures in terms of energies by setting the Boltzman constant to unity ($k_{\rm B} = 1$)

Bremsstrahlung-term, since otherwise the full core would run into a cooling catastrophe. Therefore, we can ignore the line-term in our rough estimate

$$\Lambda_X(T_{cc}) \approx \Lambda_0\, T_{cc}^{\frac{1}{2}}\,, \tag{10}$$

with $\Lambda_0 = 5.96 \cdot 10^{-24}\,\mathrm{erg\,s^{-1}\,cm^3\,keV^{-1/2}}$ (assuming a metalicity of 0.3 solar).

3.3. Hydrodynamical turbulence injection

We assume that the injection from radio galaxies is the dominant heating mechanism. Although radio galaxies certainly inject energy not all of this is in form of turbulence. During the very initial phase of inflation of a radio bubble there are shocks, which can heat the environment (Heinz et al. 1998; Fabian et al. 2003a). Later on, a series of sound waves are produced, which might be dissipated through viscosity in the medium[7]. In any case, when a radio bubble raises buoyantly in the cool core atmosphere, the environmental gas is flowing around it, which leads to injection of kinetic energy from the central radio galaxy into the cool core. The time averaged turbulence power of the source is

$$L_T = f_T\, L_{cc} = \eta_T\, L_{rg}, \tag{11}$$

where f_T is the fraction of cool core heating done by turbulence, $\eta_T \le 1$ is the efficiency of kinetic energy transfer between the injected radio plasma and the cool core gas, and L_{rg} is the mechanical luminosity of the radio galaxy ($P\,dV$ work per time). Churazov et al. (2002) argue that the efficiency factor η_T should be of the order one since the radio plasma looses most of its energy by adiabatic expansion during its buoyant rise through one scale-height of the cluster atmosphere. This energy is transfered mechanically to the kinetic energy of the ICM gas and is finally dissipated into heat. It is controversial if most of this energy is dissipated within the cool core, or within the outer regions of the cluster. Here, we assume the former and set $\eta_T = f_T = 0.5$ allowing also non-turbulent heating (shock waves, sound waves, heat transport). However, we also provide the scaling of our results with these parameters.

The injected kinetic energy is dissipated through a Kolmogorov-cascade within an eddy turnover-time

$$\tau_T \sim \lambda_T / \mathrm{v}_T\,, \tag{12}$$

where λ_T and v_T are the turbulence injection scale and turbulence root mean square velocity, respectively. The average turbulent energy of the cool core $E_T = M_{cc}\,\mathrm{v}_T^2/2$ is therefore

$$E_T = L_T\, \tau_T \approx f_T\, L_{cc}\, \lambda_T/\mathrm{v}_T\,, \tag{13}$$

yielding

$$\frac{\mathrm{v}_T^3}{\lambda_T} = \frac{2\, f_T\, L_{cc}}{M_{cc}} = \frac{2\, f_T\, L_{cc}}{m_p\, n_{cc}\, V_{cc}}\,. \tag{14}$$

This would allow the determination of the turbulent velocity and energy density if the turbulent injection scale were known. In the following, we attempt a rough estimate of the expected turbulent length scale λ_T.

3.4. Hydrodynamical turbulence injection scale

In the picture adopted for this work, the turbulence is stirred by the movement of buoyant radio plasma bubbles. The turbulence injection scale should therefore be of the order of the radius r_{bub} of the bubbles, which we approximate to be spheres. Assuming an ultra-relativistic equation of state for the radio plasma, we find the volume of the bubble is given as

$$V_{bub} = E_{bub}/(4\,P)\,, \tag{15}$$

where

$$E_{bub} = L_{rg}\,\tau_{bub}/2 = f_T L_{cc}\,\tau_{bub}/(2\,\eta_T) \tag{16}$$

is the mechanical energy released by the radio galaxy into a bubble during the time τ_{bub} the bubble needs to leave the cool core buoyantly. If the turbulence stirring bubbles were filled mostly by thermal gas, the volume of the bubble would be $V_{bub} = 2\,E_{bub}/(5\,P)$, which would make some difference to our estimates, but none which is changing the order of magnitude of our results.

The time available for the jets to inflate the bubble is its rise time through the cool core

$$\tau_{bub} \sim \frac{r_{cc}}{v_{bub}} \sim \left(\frac{r_{cc}}{r_{bub}}\right)^{\frac{1}{2}} \frac{r_{cc}}{2\,c_s}\,, \tag{17}$$

and can be estimated from the balance of drag and buoyance forces (e.g. Enßlin & Heinz 2002).

Combining Eq. 15, 16, and 17 yields the bubble radius

$$r_{bub} = \left(\frac{3\, f_T\, L_{cc}\, r_{cc}^{3/2}}{64\,\pi\,\eta_T\, c_s\, P_{cc}}\right)^{\frac{2}{7}}\,, \tag{18}$$

and thereby the required hydrodynamical turbulence scale $\lambda_T \sim r_{bub}$. Using this and the derived relations above, the turbulent velocity calculates as

$$\begin{aligned} \mathrm{v}_T &= \frac{3^{\frac{1}{21}}\,\eta_T^{\frac{1}{3}}\,\Lambda_0^{\frac{3}{7}}\,n_{cc}^{\frac{3}{7}}\,r_{cc}^{\frac{3}{7}}\,T_{cc}^{\frac{1}{14}}}{2^{\frac{4}{21}}\,5^{\frac{1}{21}}\,f_T^{\frac{1}{3}}\,m_p^{\frac{2}{7}}} \\ &= 173\,\mathrm{km/s}\left(\frac{\eta_T}{f_T}\right)^{\frac{1}{3}}\left(\frac{n_{cc}}{0.1\,\mathrm{cm^{-3}}}\right)^{\frac{3}{7}}\left(\frac{r_{cc}}{10\,\mathrm{kpc}}\right)^{\frac{3}{7}}\left(\frac{T_{cc}}{\mathrm{keV}}\right)^{\frac{1}{14}}\,, \end{aligned} \tag{19}$$

and thus, the turbulent energy density is given by

$$\varepsilon_T = \frac{3^{\frac{2}{21}}\,\eta_T^{\frac{2}{3}}\,\Lambda_0^{\frac{6}{7}}\,m_p^{\frac{3}{7}}\,n_{cc}^{\frac{13}{7}}\,r_{cc}^{\frac{6}{7}}\,T_{cc}^{\frac{1}{7}}}{2^{\frac{29}{21}}\,5^{\frac{2}{21}}\,f_T^{\frac{2}{3}}}\,. \tag{20}$$

For a number of prominent cool core clusters, Tab. 1 contains the values for v_T, $\lambda_T = r_{bub}$, and ε_T as expected from our steady-state description of cool core turbulence. Deviations due to episodic evolution of cool core turbulence are possible and expected.

[7] Pringle (1989); Churazov et al. (2001); Reynolds et al. (2002); Fujita et al. (2004); Ruszkowski et al. (2004); Reynolds et al. (2005)

3.5. Magnetic turbulence

The energy density of the magnetic turbulence ε_B is lower by a factor $f_B \sim 0.05\ldots0.2$ than the kinematic one $\varepsilon_{\rm T}$. The length-scale is also smaller by a factor $R_{\rm c}^{-1/2}$. The root-mean-square magnetic field strength in the cool core is therefore given by

$$B_{\rm rms} \;=\; \sqrt{8\,\pi\,\varepsilon_{\rm T}\,f_B} = \frac{2^{\frac{17}{21}}\,3^{\frac{1}{21}}\pi^{\frac{1}{2}}\,\eta_{\rm T}^{\frac{1}{3}}\,\Lambda_0^{\frac{3}{7}}\,m_{\rm p}^{\frac{3}{14}}\,n_{\rm cc}^{\frac{13}{14}}\,r_{\rm cc}^{\frac{3}{7}}\,T_{\rm cc}^{\frac{1}{14}}}{5^{\frac{1}{21}}\,f_{\rm T}^{\frac{1}{3}}\,R_{\rm c}^{\frac{3-d}{4}}} \qquad (21)$$

$$= \begin{cases} 5.6\,\mu{\rm G}\,\left(\frac{\eta_{\rm T}}{f_{\rm T}}\right)^{\frac{1}{3}}\left(\frac{n_{\rm cc}}{0.1\,{\rm cm^{-3}}}\right)^{\frac{13}{14}}\left(\frac{r_{\rm cc}}{10\,{\rm kpc}}\right)^{\frac{3}{7}}\left(\frac{T_{\rm cc}}{\rm keV}\right)^{\frac{1}{14}}\left(\frac{R_{\rm c}}{20}\right)^{-\frac{1}{2}} \\ 10\,\mu{\rm G}\,\left(\frac{\eta_{\rm T}}{f_{\rm T}}\right)^{\frac{1}{3}}\left(\frac{n_{\rm cc}}{0.1\,{\rm cm^{-3}}}\right)^{\frac{13}{14}}\left(\frac{r_{\rm cc}}{10\,{\rm kpc}}\right)^{\frac{3}{7}}\left(\frac{T_{\rm cc}}{\rm keV}\right)^{\frac{1}{14}}\left(\frac{R_{\rm c}}{35}\right)^{-\frac{1}{4}} \end{cases}$$

in our flux rope ($d = 1$) and magnetic sheet ($d = 2$) scenarios, respectively. The magnetic autocorrelation length is

$$\lambda_B \;=\; \frac{\lambda_{\rm T}}{R_{\rm c}^{\frac{1}{2}}} = \frac{3^{\frac{1}{7}}\,\Lambda_0^{\frac{2}{7}}\,m_{\rm p}^{\frac{1}{7}}\,n_{\rm cc}^{\frac{2}{7}}\,r_{\rm cc}^{\frac{9}{7}}}{2^{\frac{11}{7}}\,5^{\frac{1}{7}}\,R_{\rm c}^{\frac{1}{2}}\,T_{\rm cc}^{\frac{2}{7}}} \qquad (22)$$

$$= \;0.53\,{\rm kpc}\left(\frac{n_{\rm cc}}{0.1\,{\rm cm}^{-3}}\right)^{\frac{2}{7}}\left(\frac{r_{\rm cc}}{10\,{\rm kpc}}\right)^{\frac{9}{7}}\left(\frac{T_{\rm cc}}{\rm keV}\right)^{-\frac{2}{7}}\left(\frac{R_{\rm c}}{20}\right)^{-\frac{1}{2}}$$

3.6. Predicting an observable: RM dispersion

Knowing the depth of the Faraday screen $r_{\rm cc}$, the magnetic field strength $\langle B^2\rangle$, and the magnetic autocorrelation length λ_B allows to predict the expected dispersion of the Faraday rotation measure from a central radio source[8], assuming an isotropic distribution of magnetic field strengths with the help of Eq. 40 of Enßlin & Vogt (2003):

$$\langle RM^2\rangle \;=\; \frac{1}{2}\,a_0^2\,n_{\rm cc}^2\,r_{\rm cc}\,\lambda_B\,\langle B^2\rangle \qquad (23)$$

$$= \frac{3^{\frac{5}{21}}\pi\,a_0^2\,\eta_{\rm T}^{\frac{2}{3}}\,\Lambda_0^{\frac{8}{7}}\,m_{\rm p}^{\frac{4}{7}}\,n_{\rm cc}^{\frac{29}{7}}\,r_{\rm cc}^{\frac{22}{7}}}{2^{\frac{20}{21}}\,5^{\frac{5}{21}}\,f_{\rm T}^{\frac{2}{3}}\,R_{\rm c}^{2-\frac{d}{2}}\,T_{\rm cc}^{\frac{1}{7}}} \qquad (24)$$

$$RM_{\rm rms}^{\rm exp} \;=\; \begin{cases} \frac{739}{\rm m^2}\,\left(\frac{\eta_{\rm T}}{f_{\rm T}}\right)^{\frac{1}{3}}\left(\frac{n_{\rm cc}}{0.1\,{\rm cm^{-3}}}\right)^{\frac{29}{14}}\left(\frac{r_{\rm cc}}{10\,{\rm kpc}}\right)^{\frac{11}{7}}\left(\frac{T_{\rm cc}}{\rm keV}\right)^{-\frac{1}{14}}\left(\frac{R_{\rm c}}{20}\right)^{-\frac{3}{4}} \\ \frac{1180}{\rm m^2}\,\left(\frac{\eta_{\rm T}}{f_{\rm T}}\right)^{\frac{1}{3}}\left(\frac{n_{\rm cc}}{0.1\,{\rm cm^{-3}}}\right)^{\frac{29}{14}}\left(\frac{r_{\rm cc}}{10\,{\rm kpc}}\right)^{\frac{11}{7}}\left(\frac{T_{\rm cc}}{\rm keV}\right)^{-\frac{1}{14}}\left(\frac{R_{\rm c}}{35}\right)^{-\frac{1}{2}} \end{cases}$$

The two cases correspond to filamentary and sheet like magnetic structure scenarios, respectively. Here, $a_0 = e^3/(2\pi\,m_e^2\,c^4)$ is the usual Faraday rotation constant[9].

[8] Background sources should have twice the variance $\langle RM^2\rangle$ given here due to the doubled screen depth.

[9] Eq. 23 differs from the usually used, but inaccurate *RM* dispersion formula, which is based on the cell model for the magnetic fields

$$\langle RM^2\rangle \approx \frac{1}{3}\,a_0^2\,n_{\rm cc}^2\,r_{\rm cc}\,\lambda_{RM}\,\langle B^2\rangle$$

First, the proper magnetic autocorrelation length λ_B is used in Eq. 23, which differs in a non-trivial way – since this is magnetic power-spectrum dependent – from the *RM* autocorrelation length $\lambda_{\rm RM}$ derived from *RM* maps. Usually, $\lambda_{RM} > \lambda_B$. Second, the numerical factor $\frac{1}{2}$ in Eq. 23 takes properly account for the effect of the constraint $\boldsymbol{\nabla}\cdot\boldsymbol{B} = 0$, whereas for the above Eq., uncorrelated patches with internally constant magnetic fields were assumed, which do not have $\boldsymbol{\nabla}\cdot\boldsymbol{B} = 0$ at the patch boundaries. Due to the differences, published magnetic field values based on the above Eq. does not need be accurate, although the two errors partly compensate each other.

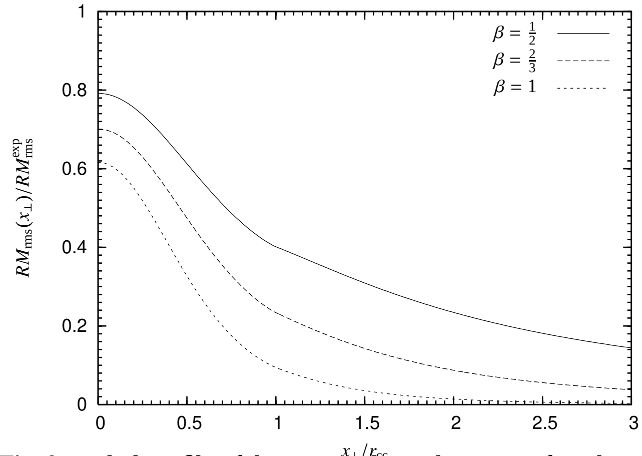

Fig. 2. Radial profile of the expected *RM* dispersion for a line of sight starting in the midplane of a β-profile cool core, but being displaced from the cluster centre by $x_\perp$. The *RM* dispersion is given in units of our result $RM_{\rm rms}^{\rm exp}$ in Eq. 23 for the solid sphere model of the cool core.

It is worth noting that the scaling of the Faraday dispersion, which can approximately be written as $RM_{\rm rms}^{\rm exp} \propto n_{\rm cc}^2\,r_{\rm cc}^{3/2}\,T_{\rm cc}^0$, is sufficiently similar to that of the bolometric luminosity of the cool core $L_{\rm cc} \propto n_{\rm cc}^2\,r_{\rm cc}^3\,T_{\rm cc}^{1/2}$ and also to the mass deposition rate $\dot{M} \propto L_{\rm cc}/T_{\rm cc} \propto n_{\rm cc}^2\,r_{\rm cc}^3\,T_{\rm cc}^{-1/2}$ to expect significant correlations, which are indeed observed (e.g. Taylor et al. 2002).

3.7. Approximate treatment of the cool core structure

In the following, we generalise the simplified geometry of a homogeneous cool core to one which has a radial structure. This generalisation allows us to predict the radial dependence of the various quantities and to test if our predictions of the central *RM* dispersion are expected to change significantly due to the contribution from radii outside the cool core radius.

In order to provide a radial dependent geometry, we make an additional assumption about the radial balance between heating and cooling. We assume that the cool core is settled in an hydrodynamical state, where heating and cooling are balanced locally at all radii below the cooling radius. Note that this does not necessarily need to be true, since in a convecting system the location of heat deposition and radiative cooling can differ, but for the sake of simplicity, we use this approximation.

The cool core is divided into spherical shells of thickness dr, which have a volume $dV(r) = 4\,\pi\,r^2\,dr$ and a luminosity $dL(r) = \Lambda_{\rm X}(T_{\rm cc})\,n_{\rm cc}^2\,dV(r)$. Our arguments about the balance of turbulent heating and radiative cooling made in Sect. 3.3 can be identically applied to each of these shells individually, leading to a relation equivalent to Eq. 14:

$$\frac{{\rm v}_{\rm T}^3(r)}{\lambda_{\rm T}(r)} = \frac{2\,f_{\rm T}}{m_{\rm p}\,n_{\rm cc}}\,\frac{dL}{dV}(r)\,. \qquad (25)$$

To derive the local turbulence injection scale, we use again the local characteristic buoyancy time $\tau_{\rm bub}(r) \sim r/v_{\rm bub}(r)$ to predict the bubble size at any cluster radius $r > r_{\rm cc}$. For $r \leq r_{\rm cc}$, we use $r_{\rm cc}$ to treat the central flat density profile properly. In doing so, we find that the replacement

$$r_{\rm cc} \rightarrow \max(r_{\rm cc}, r) \tag{26}$$

in any former equation describing local properties as in Eqs. 18-23 gives the appropriate function of radius r. Of special interest may be the expected radial scaling of the typical magnetic field strength: $B_{\rm rms} \propto n_{\rm e}^{13/14}(r)\, r^{3/7}$ which is usually a decreasing function of the radius due to the steepness of the electron profiles. For example for $n_{\rm e} \propto r^{-2}$ (and $T(r) \approx const$) we find $B_{\rm rms} \propto r^{-10/7} \propto n_{\rm e}^{5/7}$ which lies well within the range of usually assumed magnetic field scaling with electron density $B_{\rm rms} \propto n_{\rm e}^{0.5...1}$ (e.g. Dolag et al. 2001).

Global quantities like the energy content, the luminosity of a volume, etc. are calculated by performing the appropriate volume integrals. The increase of the Faraday dispersion along the line of sight should therefore be given by the differential analogy to Eq. 23

$$\frac{d\langle RM^2\rangle}{dl} = \frac{1}{2}\, a_0^2\, n_{\rm cc}^2\, \lambda_B\, \langle B^2\rangle \tag{27}$$

$$= \frac{3^{\frac{5}{21}}\pi\, a_0^2\, \eta_{\rm T}^{\frac{2}{3}}\, \Lambda_0^{\frac{8}{7}}\, m_{\rm p}^{\frac{4}{7}}\, n_{\rm e}^{\frac{29}{7}}(r)\, \max^{\frac{15}{7}}(r_{\rm cc}, r)}{2^{\frac{20}{21}}\, 5^{\frac{5}{21}}\, f_{\rm T}^{\frac{2}{3}}\, R_{\rm c}^{2-\frac{d}{2}}\, T_{\rm e}^{\frac{1}{7}}(r)}\,, \tag{28}$$

which reduces to the former result given by Eq. 24 if integrated over a cool core sphere with constant properties within $r_{\rm cc}$.

Eq. 28 allows us to check under which conditions our constant core model gives appropriate results, and under which conditions the *RM* contributions from larger radii become essential.

For an electron density profile described by the usual β-model,

$$n_{\rm e}(r) = n_{\rm cc}\left(1 + \frac{r^2}{r_{\rm cc}^2}\right)^{-\frac{3}{2}\beta}, \tag{29}$$

we find that the contribution to the *RM* dispersion per logarithmic radius peaks around the core radius $r_{\rm cc}$ if $\beta > 0.25$ (a similar statement can be made for the cool core dominating the X-ray emissivity if $\beta > 0.5$). Since typical cluster electron density profiles are described by $\beta \geq 0.5$, our ignorance of contributions of outer regions to the *RM* dispersion only introduces a moderate error of the order of 20 – 40% (depending on β) for line of sights starting in the cluster centre. Off-centre line-of sights, which often occur for extended radio lobes in our sample, will result in significantly lower *RM* dispersions. This can be seen in Fig. 3.7, where numerically estimated *RM*-profiles are shown.

We note that typical pairs of radio lobes are not located in the midplane of the cluster. One lobe has a shorter and one has a longer line-of-sight through the Faraday-active medium. In a spherical geometry of the cluster gas, the additionally accumulated $\langle RM^2\rangle$ of the back lobe, and the missing of the front lobe should compensate roughly in an average over both lobes, provided both lobes are in mirror symmetric positions with respect to the cluster centre. Therefore, in such a case the midplane *RM* dispersion is a good reference point.

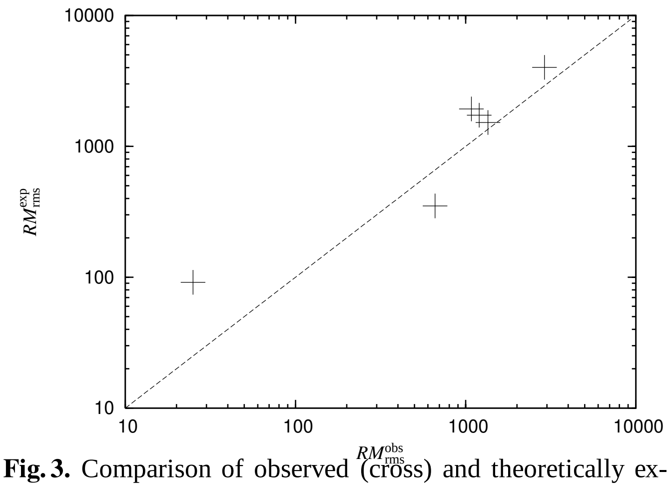

Fig. 3. Comparison of observed (cross) and theoretically expected (case $d = 1$, $R_{\rm c} = 20$) (dashed line) root-mean-squared *RM* signal. Note, that the expected *RM* is calculated for a radio source located at the centre of the cluster, whereas most *RM* measurements are somewhat off centre, probably leading to a reduced observed signal.

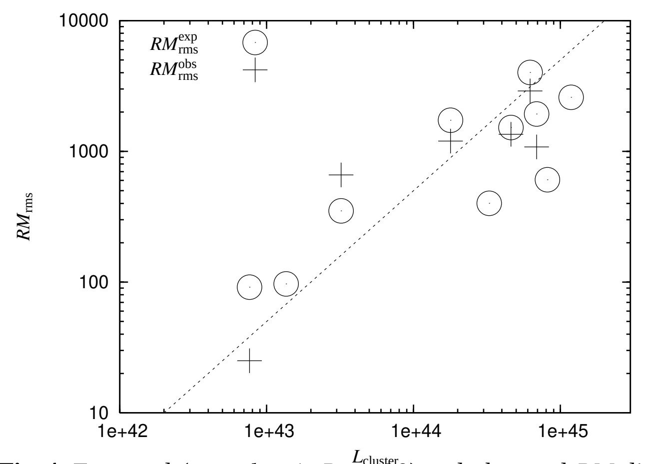

Fig. 4. Expected (case $d = 1$, $R_{\rm c} = 20$) and observed *RM* dispersion values versus the bolometric cluster luminosity. A linear correlation is also shown to guide the eye.

4. Application to Cool Cores

In the following, we apply our model to a number of cool core clusters. The input parameters of our calculations are the central electron density $n_{\rm cc}$, the central gas temperature $T_{\rm cc}$, and the core radius $r_{\rm cc}$ of the cool core. The numbers are taken from the literature and the corresponding references are given in the sections on individual clusters below. The cluster parameters and the derived properties are summarised in Tab. 1. A detailed discussion of the individual datasets of the different clusters can be found in Appendix A.

As a consistency check for the used radii of the cool cores, we calculate the emissivity $L_{\rm cc}$ within the cool core according to Eq. 8 and compare this to the reported bolometric X-ray luminosity of the complete cluster $L_{\rm cluster}$. The fraction of X-ray luminosity which is due to the cool core is in the range of $L_{\rm cc}/L_{\rm cluster} = 1\% - 50\%$. The typical fractional luminosity

cluster properties	Hydr.	Cent.	Cygn.	A1958	A2597	3C31	Pers.	A85	A2199	Virgo
n_{cc} $[10^{-3}\,/\mathrm{ccm}]$	56.1	80.6	153	189	73.5	180	50.8	30.8	33.7	151
T_{cc} [keV]	2.7	2.2	6.5	3.7	1.3	0.7	3	5.5	1.6	1
r_{cc} [kpc]	35.5	8.57	10.7	13.4	28	1.2	57	45	29	1.6
$\mathrm{RM}^{\mathrm{obs}}_{\mathrm{rms}}$ $[\mathrm{m}^{-2}]$	1350	660	1200	2900	1080	25	–	–	–	–
L_{cluster} $[10^{44}\,\mathrm{erg/s}]$	4.61	0.32	1.79	6.22	6.89	0.077	11.8	8.16	3.28	0.14
$L(< r_{\mathrm{cooling}})/L_{\mathrm{cluster}}$	0.52	0.41	0.49	–	0.61	–	0.59	0.3	0.47	0.5
$L_{\mathrm{cc}}/L_{\mathrm{cluster}}$	0.37	0.14	0.3	0.2	0.14	0.0045	0.51	0.18	0.078	0.005
hydrodynamical turbulence										
$\lambda_B \sim r_{\mathrm{bub}}$ [kpc]	7.68	1.45	1.7	2.84	7.52	0.2	13.3	7.15	5.94	0.25
ε_{T} $[10^{-10}\,\mathrm{erg/ccm}]$	0.29	0.16	0.76	1.27	0.35	0.12	0.37	0.13	0.089	0.11
v_{T} [km/s]	250	156	244	283	240	87.5	295	225	177	94
magnetic turbulence	$d = 1$ $R_{\mathrm{c}} = 20$									
λ_B [kpc]	1.72	0.32	0.38	0.64	1.68	0.045	2.97	1.6	1.33	0.056
B_{rms} $[\mu\mathrm{G}]$	6.06	4.55	9.78	12.6	6.68	3.8	6.82	4.04	3.34	3.74
κ_{visc} $[10^{27}\,\mathrm{cm}^2/\mathrm{s}]$	7.89	0.93	1.71	3.31	7.43	0.073	16.1	6.61	4.33	0.097
$\mathrm{RM}^{\mathrm{exp}}_{\mathrm{rms}}$ $[\mathrm{m}^{-2}]$	1520	351	1730	4010	1930	91.5	2590	607	400	96.9
$\mathrm{RM}^{\mathrm{obs}}_{\mathrm{rms}}/\mathrm{RM}^{\mathrm{exp}}_{\mathrm{rms}}$	0.89	1.88	0.69	0.72	0.56	0.27	–	–	–	–
magnetic turbulence	$d = 2$ $R_{\mathrm{c}} = 35$									
λ_B [kpc]	1.3	0.25	0.29	0.48	1.27	0.034	2.25	1.21	1	0.042
B_{rms} $[\mu\mathrm{G}]$	11.1	8.36	18	23.2	12.3	6.99	12.5	7.44	6.13	6.88
$\mathrm{RM}^{\mathrm{exp}}_{\mathrm{rms}}$ $[\mathrm{m}^{-2}]$	2430	561	2770	6420	3090	146	4140	970	640	155
$\mathrm{RM}^{\mathrm{obs}}_{\mathrm{rms}}/\mathrm{RM}^{\mathrm{exp}}_{\mathrm{rms}}$	0.55	1.18	0.43	0.45	0.35	0.17	–	–	–	–

Table 1. Application of the model to cool cores of the Hydra A (Hydr.), Centaurus (Cent.), Cygnus A (Cygn.), A1985, A2597, 3C31, Perseus (Pers.), A85, A2199 and Virgo clusters of galaxies. The first part of the table contains the cluster parameters whose values were taken from the literature. References and comments on possible biases of the data are given in Sect. 4 and in detail in Appendix A. The second part describes the expected hydrodynamical turbulence. The third and fourth part describe the expected magnetic turbulence for the scenarios of magnetic flux ropes ($d = 1$) and flux sheets ($d = 2$), respectively.

within the cooling radius, which is defined by the gas having a cooling time less than the Hubble time, was estimated by Peres et al. (1998). Since the cooling radius is larger than the core radius of the cool core a systematic difference is expected, and indeed found since $L(< r_{\mathrm{cooling}})/\mathrm{L}_{\mathrm{cluster}} = 40\% - 60\%$ according to Peres et al. (1998). The large differences for some clusters between the ratios are due to shallow electron density profiles with $\beta \approx 0.5$.

The other quantities in Tab. 1 are calculated according to the formulae given in Sect. 3. Only the observed rotation measure dispersion $RM^{\mathrm{obs}}_{\mathrm{rms}}$ is taken from the literature and its references are given below. Note that our expected $RM^{\mathrm{exp}}_{\mathrm{rms}}$ is calculated for a polarised synchrotron source in the middle of the cool core, whereas the real radio emitting volume may be displaced due to an inclination between radio jet and line-of-sight, and/or due to a non-central position. This will cause some deviation of our expectations from the observations and usually biases the observational values to be lower.

For a sample of cool cores with luminosities between $10^{43} - 10^{45}\,\mathrm{erg/s}$, we predict turbulent velocities in the range $100 - 300\,\mathrm{km/s}$, magnetic field strengths in the range $3 - 13\,\mu\mathrm{G}$ ($1{-}d$ scenario) or $6{-}23\,\mu\mathrm{G}$ ($2{-}d$ scenario), and Faraday dispersions in the range $100 - 4000\,\mathrm{m}^{-2}$ ($150 - 6000$ in the $2 - d$ scenario). These values should be compared to existing Faraday rotation measurements, field strength estimates, and future X-ray-spectroscopically determined velocity dispersions, as done in Tab 1, and Figs. 4 & 4. We further list our expectations for the large-scale magnetic viscosity, which we like to be regarded as speculative, and which were estimated using the calculations of Longcope et al. (2003) for an assumed $1{-}d$ flux-rope picture of the magnetic field configuration.

To summarize our results, we find that both, the one and two dimentional scenarios for the magnetic structures, predict rotation measures wich are of the same order of magnitude as the observed ones. In cases where observational estimates for field strength and lenght scxales existed, there is also a better than order of magnitude agreement. We would not expect our model to be more accurate than within a factor of two.

5. Conclusion

We showed that many properties of magnetic field measurements in cool core clusters, and especially in the case of Hydra A, which we investigate in deltail, seem to support the picture that a small-scale turbulent dynamo is maintaining the magnetic fields. Furthermore, the likely energy source of the expected turbulence are buoyant radio bubbles from the central galaxy, which can inject turbulence with the right amount of power, and also on length-scales, which fit to the observed magnetic correlation scales well.

Motivated by these indications of the physical processes in cool core clusters, we developed a steady state scenario for the hydrodynamical and magnetic turbulence, assuming that the turbulent feedback from the central radio source compensates for the cool core radiative losses. This scenario predicts turbulent length scales and energy densities which can be compared to observations.

The hydrodynamical turbulence may soon be probed with the upcoming Astro-E2 satellite mission which will allow the determination of the gas velocity dispersion (Sunyaev et al. 2003; Inogamov & Sunyaev 2003; Brüggen et al. 2005). At present, the magnetic turbulence can be tested due to the existing Faraday rotation measurements of extended radio sources in cool core clusters. The Faraday dispersion is a combined measure of the magnetic field strength and correlation length.

For a sample of prominent cool core clusters, we calculate the expected hydro- and magnetic-turbulence, and the predicted Faraday dispersion. In cases of existing Faraday measurements, we find that our estimates reproduce the observed magnitude of the dispersion over roughly two orders of magnitude in *RM* (or four in $\langle RM^2 \rangle$). On average, our predictions are a factor of two higher than the measurements, which is not too surprising, since the actual data sample larger cluster radii, whereas our estimates are aiming for a radio source at the cluster centre.

The critical reader might wonder about the amount of fine tuning which went into our model. The answer is nearly none, but this is probably a mere coincidence rather than a prove for the investigated scenario. There are various places in the calculation where factors of order one could or should have been introduced. One example is the assumption of the bubble radius being exactly the turbulence injection scale. This assumption will require verification by numerical simulations of the hydrodynamics, which is well beyond the scope of this initial investigation. Another uncertain area are the adopted parameters of the dynamo theory, which are also not fully settled in the literature.

Nevertheless, we have shown that the straight-forward application of current concepts of turbulent magnetic dynamos in combination with the emerging picture of cool core stabilisation via heat injection due to the dissipation of turbulence seeded by radio galaxy feedback leads to expectations for the Faraday rotation signal which match well with the observed ones. This is the case for a variety of galaxy clusters spanning two orders of magnitude in their X-ray luminosities. Therefore, our picture of cluster cool core heating by radio galaxy feedback and the theory of turbulent magnetic dynamos passed a critical test.

Acknowledgements. We acknowledge stimulating discussions with K. Subramanian and A. Schekochihin on the theory of small-scale dynamos. We are thankful to R. Laing to provide us with the results on 3C31 prior to publication, and to V. Springel and E. Churazov for comments on the manuscript.

Appendix A: Individual clusters

A.1. Hydra A cluster

The gas parameters for the Hydra A cluster are taken from Mohr & Evrard (1997), and the X-ray luminosity is provided by Ikebe et al. (1997). The first detailed *RM* map of Hydra A was published by Taylor & Perley (1993), which exhibited very large *RM* values, especially for the south lobe of Hydra A. The data was reanalysed using the PACERMAN algorithm (Dolag et al. 2005; Vogt et al. 2005), which removed all areas in the northern-lobe, and many of the southern-lobe with extremely high *RM* values, indicating that those were observational artefacts. Since the southern lobe *RM* data seem to be still contaminated by observational artefacts, as statistical tests for anti-correlations of gradients of polarisation angles and *RM* values reveal (Enßlin et al. 2003), we use only the dispersion of the northern lobe, as reported by Vogt et al. (2005). The same *RM* map was analysed by Vogt & Enßlin (2005) using a maximum-likelihood power spectra estimator (see Fig. 1), revealing central magnetic field strength of $B_{\rm rms} \approx 7\,\mu$G with an autocorrelation length of $\lambda_B \approx 3$ kpc.

We note that model expectations and observational values of Faraday dispersion, magnetic field strength, and autocorrelation length agree well. Since the Hydra A north lobe is known to approach the observer (and the radio emission extend to larger radii), the observational *RM* dispersion should be a bit biased to lower values.

A.2. Centaurus cluster

The central electron density and the cool core radius are taken from Mohr et al. (1999)[10], and the central temperature from White (2000)[11]. The observed Faraday dispersion for the Centaurus cluster is derived from the embedded radio source PKS 1246-410 by Taylor et al. (2002). The published Faraday rotation map reveals several isolated patches of extreme *RM* values, and a histogram of *RM* values exhibits multiple peaks. A statistical analysis of the alignment of *RM* gradients and polarisation angle gradients reveals a significant anti-correlation between the two (Enßlin et al. 2003), which is also an indication of observational artefacts in this map. Thus, the reported *RM* dispersion may be too large. However, an order of magnitude agreement between observed and expected *RM* dispersion is found.

Taylor et al. (2002) report a *RM*-correlation length of $\lambda_{RM} \sim 0.7$ kpc and a field strength of $9\,\mu$G, which is significantly different from our expectations. The different length scale is not surprising, since usually $\lambda_{RM} > \lambda_B$ (Enßlin & Vogt 2003). The larger observationally derived magnetic field strength may be a result of the very small core radius and/or the possible overestimate of the *RM* dispersion reported in Taylor et al. (2002).

To summarise, the X-ray and radio observational data of the cool core of the Centaurus cluster would need further improvements before conclusive statements about an agreement or disagreement of our model and observations can be made in this case. Both, the observed and the expected *RM* dispersion could be subject to re-adjustments. We like to stress that the complex morphology of this cool core is probably causing the

[10] Using the extremely small core radius given in Taylor et al. (2002) leads to a cool core fractional luminosity of only 3%, which is obviously much smaller than the 40% observed (Peres et al. 1998).

[11] Lower central temperatures have been reported by Sanders & Fabian (2002) and Taylor et al. (2002), but since they were not used for the electron density estimates, and since our magnetic field and *RM* predictions are quite insensitive to the temperature, we do not use them.

difficulties to single out a *'real'* core radius and central electron density.

A.3. Abell 1958 cluster (3C295)

The electron density, central temperature, cool core radius, and dispersion measure are taken from Allen et al. (2001) and the cluster luminosity from Allen et al. (2003).

The agreement of predicted and observed Faraday dispersion is very good. Furthermore, the rather high predicted magnetic field strength of $10 - 20\,\mu$G is also found observationally, since Allen et al. (2001) report $14\,\mu$G.

A.4. Cygnus A cluster

We use the electron density, temperature, and cool core radius reported in Mohr et al. (1999). We measure the *RM* dispersion to be $1200\,\mathrm{m}^{-2}$ from the map published by Dreher et al. (1987) after removing pixels from the map with extraordinary large *RM* jumps, which we associate with observational artefacts ($n\pi$-ambiguities). Similar to the case of Hydra A, we see an asymmetry in the *RM* dispersion between the two lobes, which is a consequence of the different depth of the lobes (the Laing-Garrington effect: Laing 1988; Garrington et al. 1988). Unfortunately, the two radio lobes are located well beyond the cool core radius, which is even more true for their polarised regions used for *RM* measurements. Since we expect a declining magnetic-field strength as a function of radius, the reported *RM* dispersion is likely smaller than the one, which would be measured from a radio source located in the centre of the cool core, as discussed in Sect. 3.7 and illustrated in Fig. 3.7. The predicted central *RM* dispersion is a factor of two smaller than the peripherally measured one. With our current understanding of the geometry, it is fair to say that there is no apparent conflict between these numbers.

A.5. Perseus cluster

We take the central electron density, temperature, and the cool core radius from Churazov et al. (2003) and the cluster X-ray luminosity from David et al. (1993).

The Perseus cluster cool core exhibits diffuse radio emission, a radio mini-halo. One can apply the classical minimum-energy arguments to the radio halo data to search for the minimum of the sum of the magnetic and relativistic particle energy densities necessary to reproduce the radio synchrotron emission, and assume a constant proton to electron ratio k_p. Pfrommer & Enßlin (2004) report a classical minimum field strength of $7.2^{+4.5}_{-0.4}\,\mu$G (assuming $k_\mathrm{p} = 1$), where the *confidence interval* is given by the requirement that the energy density should be within one e-fold from the minimum. Pfrommer & Enßlin (2004) also develop and apply the hadronic minimum-energy criteria to the Perseus mini-halo. This criterion assumes that the relativistic electrons are injected by hadronic interactions of a relativistic proton population, which usually dominates the relativistic energy budget. No proton-to-electron factor k_p has to be assumed in this case, since the physics of the hadronic interaction determines this ratio. Applied to the Perseus radio halo, a very similar central field strength of $8.8^{+13.8}_{-5.4}\,\mu$G was found. Our cool core model predicts a field strength of $7 - 13\,\mu$G, which is well in agreement with these findings. A significant lower central field value of about $1 - 3\,\mu$G was reported by Sanders et al. (2005), based on an Inverse Compton interpretation of a hard photon component in the X-ray spectra of the cool core region. Note, that if the hard photons flux would be due to another physical mechanism, the derived value will become a lower limit. If the Inverse Compton nature of the flux could be verified, this will be a very good field estimate in case of a non-intermittent field distribution. If there is significant magnetic intermittency, spatially inhomogeneous electron cooling can produce an anti-correlation between fields and relativistic electrons, which can easily lead to Inverse Compton based magnetic field estimates lower by a factor of two (Enßlin et al. 1999; Enßlin 2004).

As stated before, Fabian et al. (2003b) argued for a large-scale viscosity in the Perseus cluster cool core of at least $4 \cdot 10^{27}\,\mathrm{cm}^2/\mathrm{s}$, which is in good agreement with the $1.6 \cdot 10^{28}\,\mathrm{cm}^2/\mathrm{s}$ predicted in our $1 - d$ scenario.

A.6. Abell 2597

This cool core galaxy cluster has been observed with Chandra by McNamara et al. (2001). This observation has been reanalysed recently by Pollack et al. (2005). The gas parameters are taken from this reanalysis. The total luminosity used is taken from David et al. (1993).

Pollack et al. (2005) study also the polarisation properties of the central radio source in this cluster. They determine a *RM* dispersion of 1080 rad m^{-2} comparable to our expectations. They conclude that the cluster magnetic field has a minimum magnetic field strength of $2.1\,\mu$G. Our model predicts a higher magnetic field strength of 7-12 μG which is in agreement with the lower limit of Pollack et al. (2005).

A.7. 3C31

The cool X-ray environment of the extended radio source 3C31 is associated with a group of galaxies. X-ray measurements suggest that this group shows properties similar to a cool core of a galaxy cluster. Therefore, it seems to be a good case to test our model in a different situation. The parameters for the gas were taken from Hardcastle et al. (2002). However we use the total luminosity from Komossa & Böhringer (1999).

Detailed *RM* measurements have been carried out by Laing et al. (in prep.). They determine the *RM* dispersion to be 25 rad m^{-2} (Laing, private communication).

A.8. Abell 85

We use the electron density, temperature, cool core radius, and luminosity reported in Mohr et al. (1999), and David et al. (1993). To our knowledge, no *RM* measurements or magnetic field estimates are available for the centre of this and all following clusters. Thus, our *RM* results are predictions.

A.9. Abell 2199

The parameters of the electron density profile as reported in Mohr et al. (1999) were used. The temperature of the cool core are taken from Voigt et al. (2002) and the total luminosity from David et al. (1993).

A.10. Virgo cluster

The Virgo cluster was observed with XMM-Newton by Matsushita et al. (2002). The gas parameters are taken from their analysis. However the total luminosity of David et al. (1993) is used for our calculations. The large difference between the cool core luminosity and the luminosity within the (larger) cooling radius is due to the extremely shallow density profile ($\beta \approx 0.5$) of Virgo. However, this should not affect our RM estimates too much, since only a $\beta \approx 0.25$ should lead to problems, as was argued above.

References

Allen, S. W. 1995, MNRAS, 276, 947
Allen, S. W., Schmidt, R. W., Fabian, A. C., & Ebeling, H. 2003, MNRAS, 342, 287
Allen, S. W., Taylor, G. B., Nulsen, P. E. J., et al. 2001, MNRAS, 324, 842
Böhringer, H., Matsushita, K., Churazov, E., Ikebe, Y., & Chen, Y. 2002, A&A, 382, 804
Bicknell, G. V., Cameron, R. A., & Gingold, R. A. 1990, ApJ, 357, 373
Brüggen, M. & Kaiser, C. R. 2001, MNRAS, 325, 676
Brüggen, M., Kaiser, C. R., Churazov, E., & Enßlin, T. A. 2002, MNRAS, 331, 545
Brandenburg, A. & Subramanian, K. 2004, ArXiv Astrophysics e-prints
Brüggen, M., Hoeft, M., & Ruszkowski, M. 2005, ArXiv Astrophysics e-prints
Carilli, C. L. & Taylor, G. B. 2002, Ann. Rev. of Astr. & Astrophys., 40, 319
Cen, R. 2005, ApJ, 620, 191
Chandran, B. D. G. 2004, ApJ, 616, 169
Chandran, B. D. G. & Maron, J. L. 2004, ApJ, 602, 170
Cho, J., Lazarian, A., Honein, A., et al. 2003, ApJL, 589, L77
Churazov, E., Brüggen, M., Kaiser, C. R., Böhringer, H., & Forman, W. 2001, ApJ, 554, 261
Churazov, E., Forman, W., Jones, C., & Böhringer, H. 2003, ApJ, 590, 225
Churazov, E., Forman, W., Jones, C., Sunyaev, R., & Böhringer, H. 2004, MNRAS, 347, 29
Churazov, E., Sunyaev, R., Forman, W., & Böhringer, H. 2002, MNRAS, 332, 729
Clarke, T. E. 2004, Journal of Korean Astronomical Society, 37, 337
Clarke, T. E., Kronberg, P. P., & Böhringer, H. 2001, ApJL, 547, L111
Crawford, C. S., Allen, S. W., Ebeling, H., Edge, A. C., & Fabian, A. C. 1999, MNRAS, 306, 857
David, L. P., Slyz, A., Jones, C., et al. 1993, ApJ, 412, 479
De Young, D. S. 1992, ApJ, 386, 464
Dennis, T. J. & Chandran, B. D. G. 2005, ApJ, 622, 205
Dolag, K., Schindler, S., Govoni, F., & Feretti, L. 2001, A&A, 378, 777
Dolag, K., Vogt, C., & Enßlin, T. A. 2005, MNRAS, 358, 726
Donahue, M., Mack, J., Voit, G. M., et al. 2000, ApJ, 545, 670
Dreher, J. W., Carilli, C. L., & Perley, R. A. 1987, ApJ, 316, 611
Edge, A. C. 2001, MNRAS, 328, 762
Edge, A. C. & Frayer, D. T. 2003, ApJL, 594, L13
Eilek, J. A. & Owen, F. N. 2002, ApJ, 567, 202
Enßlin, T. 2004, Journal of Korean Astronomical Society, 37, 439
Enßlin, T. A. & Heinz, S. 2002, A&A, 384, L27
Enßlin, T. A., Lieu, R., & Biermann, P. L. 1999, A&A, 344, 409
Enßlin, T. A. & Vogt, C. 2003, A&A, 401, 835
Enßlin, T. A., Vogt, C., Clarke, T. E., & Taylor, G. B. 2003, ApJ, 597, 870
Fabian, A. C., Nulsen, P. E. J., & Canizares, C. R. 1991, A&A Rev., 2, 191
Fabian, A. C., Sanders, J. S., Allen, S. W., et al. 2003a, MNRAS, 344, L43
Fabian, A. C., Sanders, J. S., Crawford, C. S., et al. 2003b, MNRAS, 344, L48
Feretti, L., Dallacasa, D., Giovannini, G., & Tagliani, A. 1995, A&A, 302, 680
Feretti, L., Dallacasa, D., Govoni, F., et al. 1999, A&A, 344, 472
Fujita, Y., Suzuki, T. K., & Wada, K. 2004, ApJ, 600, 650
Garrington, S. T., Leahy, J. P., Conway, R. G., & Laing, R. A. 1988, Nature, 331, 147
Ge, J. P. & Owen, F. N. 1993, AJ, 105, 778
Govoni, F. & Feretti, L. 2004, International Journal of Modern Physics D, 13, 1549
Govoni, F., Taylor, G. B., Dallacasa, D., Feretti, L., & Giovannini, G. 2001, A&A, 379, 807
Hansen, L., Jorgensen, H. E., & Norgaard-Nielsen, H. U. 1995, A&A, 297, 13
Hardcastle, M. J., Worrall, D. M., Birkinshaw, M., Laing, R. A., & Bridle, A. H. 2002, MNRAS, 334, 182
Haugen, N. E., Brandenburg, A., & Dobler, W. 2004, Phys. Rev. E, 70, 016308
Heckman, T. M., Baum, S. A., van Breugel, W. J. M., & McCarthy, P. 1989, ApJ, 338, 48
Heinz, S., Reynolds, C. S., & Begelman, M. C. 1998, ApJ, 501, 126
Hoeft, M. & Brüggen, M. 2004, ApJ, 617, 896
Ikebe, Y., Makishima, K., Ezawa, H., et al. 1997, ApJ, 481, 660
Inogamov, N. A. & Sunyaev, R. A. 2003, Astronomy Letters, 29, 791
Jaffe, W. 1980, ApJ, 241, 925
Jaffe, W. & Bremer, M. N. 1997, MNRAS, 284, L1
Johnston-Hollitt, M. & Ekers, R. D. 2004, ArXiv:astro-ph/0411045
Jubelgas, M., Springel, V., & Dolag, K. 2004, MNRAS, 351, 423
Kim, K.-T., Kronberg, P. P., & Tribble, P. C. 1991, ApJ, 379,

80
Komossa, S. & Böhringer, H. 1999, A&A, 344, 755
Laing, R. A. 1988, Nature, 331, 149
Loewenstein, M. & Fabian, A. C. 1990, MNRAS, 242, 120
Longcope, D. W., McLeish, T. C. B., & Fisher, G. H. 2003, ApJ, 599, 661
Malyshkin, L. 2001, ApJ, 554, 561
Matsushita, K., Belsole, E., Finoguenov, A., & Böhringer, H. 2002, A&A, 386, 77
Mazzotta, P., Brunetti, G., Giacintucci, S., Venturi, T., & Bardelli, S. 2004, Journal of Korean Astronomical Society, 37, 381
McNamara, B. R., Wise, M. W., Nulsen, P. E. J., et al. 2001, ApJL, 562, L149
Mohr, J. J. & Evrard, A. E. 1997, ApJ, 491, 38
Mohr, J. J., Mathiesen, B., & Evrard, A. E. 1999, ApJ, 517, 627
Narayan, R. & Medvedev, M. V. 2001, ApJL, 562, L129
Nipoti, C. & Binney, J. 2004, MNRAS, 349, 1509
O'Dea, C. P., Payne, H. E., & Kocevski, D. 1998, AJ, 116, 623
Oegerle, W. R., Cowie, L., Davidsen, A., et al. 2001, ApJ, 560, 187
Peres, C. B., Fabian, A. C., Edge, A. C., et al. 1998, MNRAS, 298, 416
Perley, R. A. & Taylor, G. B. 1991, AJ, 101, 1623
Pfrommer, C. & Enßlin, T. A. 2004, MNRAS, 352, 76
Pollack, L. K., Taylor, G. B., & Allen, S. W. 2005, ArXiv:astro-ph/0503250
Pringle, J. E. 1989, MNRAS, 239, 479
Quilis, V., Bower, R. G., & Balogh, M. L. 2001, MNRAS, 328, 1091
Reynolds, C. S., Heinz, S., & Begelman, M. C. 2002, MNRAS, 332, 271
Reynolds, C. S., McKernan, B., Fabian, A. C., Stone, J. M., & Vernaleo, J. C. 2005, MNRAS, 357, 242
Roland, J. 1981, A&A, 93, 407
Rudnick, L. & Blundell, K. M. 2003, ApJ, 588, 143
Ruszkowski, M. & Begelman, M. C. 2002, ApJ, 581, 223
Ruszkowski, M., Brüggen, M., & Begelman, M. C. 2004, ApJ, 615, 675
Ruzmaikin, A., Sokolov, D., & Shukurov, A. 1989, MNRAS, 241, 1
Salomé, P. & Combes, F. 2003, A&A, 412, 657
Sanders, J. S. & Fabian, A. C. 2002, MNRAS, 331, 273
Sanders, J. S., Fabian, A. C., & Dunn, R. J. H. 2005, ArXiv Astrophysics e-prints
Schekochihin, A., Cowley, S., Maron, J., & Malyshkin, L. 2002, Phys. Rev. E, 65, 016305
Schuecker, P., Finoguenov, A., Miniati, F., Böhringer, H., & Briel, U. G. 2004, A&A, 426, 387
Smith, E. P., Bohlin, R. C., Bothun, G. D., et al. 1997, ApJ, 478, 516
Soker, N. 2003, MNRAS, 342, 463
Soker, N. 2004, MNRAS, 350, 1015
Soker, N., Blanton, E. L., & Sarazin, C. L. 2004, A&A, 422, 445
Soker, N. & Pizzolato, F. 2005, ApJ, 622, 847
Soker, N. & Sarazin, C. L. 1990, ApJ, 348, 73
Sokolov, D. D., Ruzmaikin, A. A., & Shukurov, A. 1990, in IAU Symp. 140: Galactic and Intergalactic Magnetic Fields, 499–502
Subramanian, K. 1999, Physical Review Letters, 83, 2957
Subramanian, K., Shukurov, A., & Haugen, N. E. L. 2005, ArXiv Astrophysics e-prints
Sunyaev, R. A., Norman, M. L., & Bryan, G. L. 2003, Astronomy Letters, 29, 783
Taylor, G. B., Fabian, A. C., & Allen, S. W. 2002, MNRAS, 334, 769
Taylor, G. B., Govoni, F., Allen, S. W., & Fabian, A. C. 2001, MNRAS, 326, 2
Taylor, G. B. & Perley, R. A. 1993, ApJ, 416, 554
Tribble, P. C. 1993, MNRAS, 263, 31
Vogt, C., Dolag, K., & Enßlin, T. A. 2005, MNRAS, 358, 732
Vogt, C. & Enßlin, T. A. 2003, A&A, 412, 373
Vogt, C. & Enßlin, T. A. 2005, A&A, 434, 67
Voigt, L. M. & Fabian, A. C. 2004, MNRAS, 347, 1130
Voigt, L. M., Schmidt, R. W., Fabian, A. C., Allen, S. W., & Johnstone, R. M. 2002, MNRAS, 335, L7
White, D. A. 2000, MNRAS, 312, 663
Widrow, L. M. 2002, Reviews of Modern Physics, 74, 775
Zeldovich, Y. B., Ruzmaikin, A. A., & Sokoloff, D. D. 1990, The almighty chance (World Scientific Lecture Notes in Physics, Singapore: World Scientific Publication, 1990)